ORIGINAL PAPER

Failure height and fracture evolution pattern of overburden rock in fully mechanized cave mining

Xiaolei Wang[1] · Hu Li[2]

Abstract
With the application of a large-mining-height working face of a mine in Shanxi as the test surface, segmented water injection, borehole television and microseismic monitoring were employed to detect the damage height of overlying rock and digitally analyse the inclination of cracks before and after mining and the relationship between the number of cracks and depth, including the number of cracks and width. A similar simulation test was conducted of the fracture evolution process. The results of this study indicated that the height of the caving zone in fully mechanized cave mining reached 40.2 m, and the height of the water-conducting fracture zone reached 126.5 m. Premining fractures were dominated by high angles and small widths. Upon gradual advancement of the coal mining face, the number of cracks linearly increased, and newly formed cracks mainly exhibited low angles and moderate widths. At the early stage of mining, the number and width of cracks gradually increased with increasing advancement of the working face location. Due to the presence of overlying strata, the mined-out area could be compacted, and the number of cracks could be reduced, thus forming the characteristics of repeated cracks. During working face advancement, upon overburden collapse, cracks could appear, thereby gradually increasing the number and width of cracks. In the area near the coal wall ahead of the working face, the number of cracks remained large due to supporting pressure occurrence, and the crack density in the overburden was distributed in a snake-like pattern.

Keywords Mining engineering · Overburden failure · Crack evolution · Dynamic development

Introduction

China's coal reserves rank third in the world, and the coal output of China ranks first globally. According to the coal seam thickness, moderate-thick coal seams are the most abundant, accounting for approximately 45% of the total reserves, which is an important point in the growth of Chinese coal production (Ni et al. 2019; Li et al. 2021a; Fan and Liu 2019; Fu and Wang 2020). Coal occupies an important position in the energy structure of China and constitutes a pillar industry of the national economy. In the future, economic development of coal in China will still occupy a dominant position. Since the early 1950s, China has mined more than 36 billion tons of coal resources (Ekin 2020; Fan 2020; Tang et al. 2021; Wang et al. 2020a; Wei et al. 2021a; Zhao and Fu 2020). The large amount of coal resources makes further mining conditions more difficult. With the increasing demand for coal resources in China, the speed of coal mining is increasing, and resources encompassing shallow and deep coal seams have been nearly exhausted, resulting in coal enterprises mining deeper (Xie et al. 2019; Xia et al., 2021; Yang et al. 2020a; Kang 2020; Zuo et al. 2019). The aforementioned deep mining results in a higher gas pressure and content with a softer coal quality and lower coal seam permeability, including gas drainage difficulty and the potential for serious coal and gas outbursts. However, in recent years, many coal enterprises have pursued coal production but have neglected safety concerns, which has led to frequent coal mine accidents in China (Zhang and Wang; 2020; Su et al. 2021, 2020a; Wang et al. 2020b; Wang and Wang 2021; Wang 2019a). Gas and mine water inrush accidents are the most serious and have resulted inestimable losses to China and its people. In particular, major coal mine

✉ Xiaolei Wang
wangxiaolei@llu.edu.cn

1 Department of Mining Engineering, Luliang University, Lvliang 033000, China

2 Department of Railway Engineering, Sichuan College of Architectural Technology, Chengdu 610399, China

accidents negatively influence social stability and the development of a harmonious society, so it is urgent to strengthen gas and water inrush control in coal mines. Because of the unfavourable natural conditions of coal mines and numerous accidents, such as gas outbursts, water inrush disasters, roof collapses and fires, there occur significant hidden dangers in the process of mining working faces (Ju et al. 2020; Hu et al. 2021; Huang et al. 2015; Xu et al. 2019; Yang et al., 2020b; Zhang et al. 2020a). Among these hidden dangers, gas has become a threat to the safety of workers and coal mine economic efficiency. Among the more than 100 recorded coal mines in China, more than 70 production mines are threatened by gas hazards, which seriously affects the sustainability of production and mining life and severely restricts the development of high-yield and high-efficiency coal mines (Zhai 2015; Zhang et al. 2021; Xu and Gao 2020; Wang et al. 2021).

Regarding the prevention of mine gas, the main method of gas extraction is to drill into the coal seam and gas gathering area, connect the drilling hole to a specific pipeline and apply extraction equipment to pump gas from the coal seam and goaf to the surface to be used or discharged into the total return air stream (Ren 2020; Su et al. 2020b; Chen et al. 2021a; Cai 2020; Chai et al.2020a). Gas drainage is not only an important measure to reduce the amount of gas emissions in the process of mining but also an important measure to prevent gas from accumulating and exceeding the acceptable limit (Li et al. 2021b, 2017; Kang 2021; Liu and Wang 2018; Shi et al. 2019), thus preventing gas explosions or coal and gas outburst accidents while also ensuring the effective development and utilization of coal-associated resources (Jiang et al., 2021;Jia et al. 2018; Cheng et al. 2019; Li et al. 2020a; Li and Wang 2020). Gas drainage holes are usually arranged between the fractured and caving zones, and their placement is therefore critical for gas prevention and control to accurately obtain the failure characteristics and fracture evolution of overlying strata (Zhang et al. 2019; Zhou et al. 2021; Wang et al. 2011; Wang 2019a, b; Wei et al. 2021b; Li and Du 2020; Huang and Wu 2018).

The overlying rock mass affected by the mining stress field is referred to as the mining overlying rock mass after the extraction of underground coal resources (Ma et al., 2018; Chai et al. 2020b; Gu et al. 2019; He et al. 2014; Li et al. 2020b). The formed caving zone, fracture zone and bend zone in the mine overburden are referred to as the upper three zones. The caving zone is an irregular caving zone, with an irregular arrangement of rock blocks, as well as the highest loose coefficient (Trofimov and Shipovskii 2020; Qie et al. 2021; Hou et al. 2020a; Han 2017; Cheng et al. 2020), and the maximum caving height is determined by the unique lithology combination and rock physical and mechanical properties of the coal seam roof in the working face. Determination of the height of the caving zone is the

key to understanding the distribution of these three zones and constitutes the premise to reasonably design the strata of high-drawing roadways and final high-drawing boreholes (Pan et al. 2017; Miao et al. 2019; Hou et al. 2020b; Jiang et al. 2021b; Wang et al. 2020c). The fracture zone is the area where rock blocks remain regularly arranged after rock layer fracturing and exhibits a low expansion coefficient, which is usually denoted as the water-conducting fracture zone combined with the caving zone (Wang 2019b; Cai et al. 2014; Chen 2020; Cui et al. 2020; Gan et al. 2020; Gao 2019). Mining fissures are common in overlying strata during continuous advancement of the coal face. Because of their nature, mining fissures can be divided into vertical fracture fissures, bed-separation fissures and mining joint activation fissures. Interlayer fractures in a given rock layer entail fractures along the layer surface (Du and Wang, 2020; Fang et al. 2018; He et al. 2021; Gao 2021; Zhu et al. 2021; Zhang et al. 2020b), which emerge along the layer with rock layer sinking. These fractures can expand and deform the coal layer, thereby releasing gas pressure, causing gas to gush out of fractures in the separation layer along the gas and water passages between the upper and lower strata (Wu et al. 2021; Xia et al. 2020; Zhu et al. 2019; Zhang et al. 2014; Yin et al. 2018). The study of overburden structure damage and fracture evolution is not only important for mine water disaster control but also important for gas disaster prevention and development of coalbed methane resources (Ye et al. 2017; Yin et al. 2016; Xue et al. 2016; Xia et al. 2021; Wu et al. 2014; Zhu and Teng 2021; Hu et al. 2019).

Many scholars in China and abroad have conducted much research regarding the damage characteristics of overlying rock formations, mainly including theoretical methods, field test methods and experimental methods (Cai et al. 2020; Jia and Hu 2020; Hu et al. 2020; Liu et al. 2020). Theoretical methods are mainly based on the three-zone empirical equation for theoretical calculation purposes. These methods integrate mining technology, coal seam thickness, inclination angle and other factors influencing the height of overburden failure. Finally, in the empirical equation, the independent variable is the thickness of the coal seam. With improvement of Chinese mining technology and continuous increase in the mining height, this empirical equation is no longer suitable under the current mining conditions. Experimental methods largely include numerical simulation and similar simulation methods (Chen et al. 2021b; Ma et al. 2020; Pan et al. 2020). Regarding numerical simulation, field testing and similar simulation approaches have been significantly reduced. This is attributed to insufficiency during experiments. However, it is possible to observe the characteristics of overburden collapse and crack evolution in a more intuitive manner (Yan et al. 2020; Wu et al. 2019; Yu et al. 2021; Yuan and Xu 2019). The software used in these methods includes RFPA, UDEC, FLAC and other simulation

software packages. Although this method can significantly reduce the cost and labour intensity, actual mining conditions are hardly simulated, and there are many shortcomings in the parameters. Simulations can only be employed as an auxiliary means. Similar simulation approaches comprise an important scientific research method (Feng et al. 2017; Chen et al. 2020; Li et al. 2021b). Simulations are conducted to develop prototype models similar to laboratory experiments with a similar principle. These experiments apply test instruments to observe the mechanical parameters and distribution pattern in these models and then consider the obtained model experimental results to develop prototypes (Hu et al. 2019; Su et al. 2021). The possible mechanical phenomena and evolution of the rock mass pressure distribution are employed to solve the actual problems in rock mass engineering production. Similarity-based simulation experiments follow three similarity theorems. These theorems adhere to geometric, kinematic, and dynamic similarities (Zhai et al. 2022; Kang 2021; Fan 2020). However, when this method is applied to simulate the material ratio, the workload is high, and it is not easy to accurately formulate consistent materials. Field test methods mostly include borehole television, segmented water injection, microseismic monitoring, geological radar and other methods. However, these methods measure the failure characteristics of the overburden at certain stages but cannot continuously monitor the dynamic development process, which considerably reduces the credibility of the obtained data (Li et al. 2017; Chen et al. 2020).

Based on the above reasons, this paper adopted a mine in the Shanxi region as a test mine, thereby applying borehole television observation, drilling segmented water injection and microseismic monitoring technology to detect the height of overburden failure in the mining process of the working face, and the development of cracks during the mining process of the working face was quantified. Chemical analysis, combined with similar models to simulate the evolution characteristics of fractures, was also conducted.

Engineering conditions

The selected mine in Shanxi provides a production capacity of 6.0 Mt/a, mainly involving coal seam #3. The average thickness of this coal seam is 5.8 m. The coal seam is stable and exhibits a simple coal seam structure. The average inclination angle of the coal seam is 5°, which is nearly horizontal. In the working face test, the average buried depth of the working face reaches 415.4 m, and the direction and inclined length of the working face are 1258 m and 278 m, respectively. The coal mining technique of fully mechanized cave mining is adopted. The roof of the working face consists of fine sandstone and grey sandy mudstone. The mineralogical composition mainly includes quartz and

feldspar. The obtained core is relatively complete. The core compressive strength reaches 121.6 MPa. There occur fissures in the #3 coal seam. Nearby outcrops are formed by weathering. When broken, the compressive strength of the coal seam rock is significantly reduced, and simultaneously, the roadway at the open cut is deformed, and the pressure is increased.

Analysis of the overlying rock failure characteristics

Overburden failure height

Zonal water injection

The segmented water injection test method is a simple and accurate method to assess the damage height of the overburden (the structure of the test instrument is shown in Fig. 1). In this method, damage is bound to occur. The area near the working face is severely affected by mining, and the rock formation is notable affected due to damage. With increasing distance, the degree of damage gradually decreases, and a regular damage zone is eventually formed. The segmented water injection test method is applied to investigate the damaged area. The water injection volume in severely affected areas must be large, and vice versa. The overburden damage height is determined based on the water injection volume during drilling.

In the test process, the sealing test is performed first, the rubber sealing section is pressurized, the valve is closed, and the pressure gauge of the rubber sealing section is monitored. If no change occurs within half an hour, this
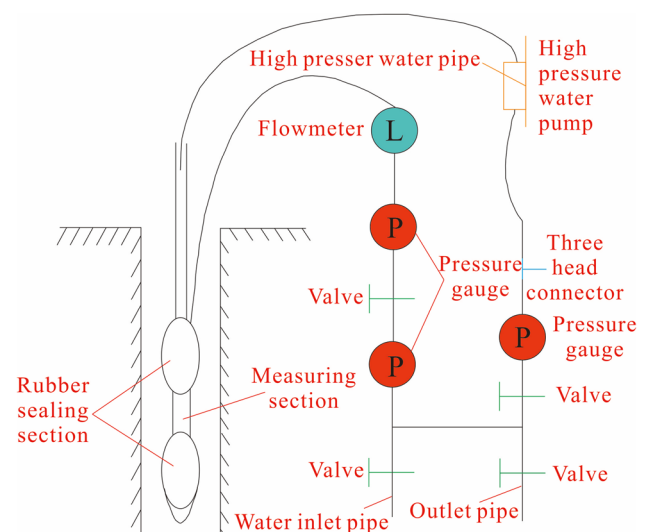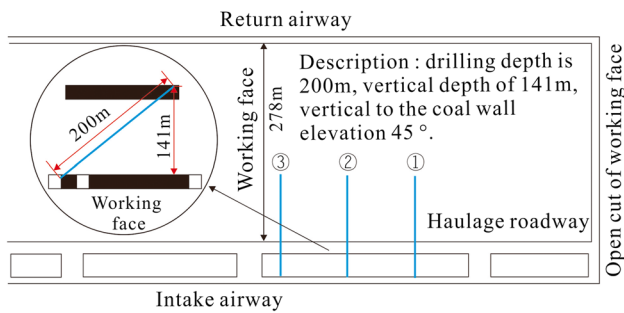

Fig. 1 Zonal water injection device

Fig. 2 Diagram of the drilling layou

indicates that the sealing effect is satisfactory. Conversely, the device is reconnected. After the sealing test, the rubber sealing section is pressurized. When the pressure remains stable, the water inlet pipe is opened, and counting is started after the flowmeter reading remains constant. Water in the sealing section is released, and the next stage of testing is initiated.

In this test experiment, three test drilling boreholes were arranged in the air inlet tunnel of the 4302 working face. The drilling length was 200 m, and the elevation angle was 45°. The drilling layout is shown in Fig. 2.

In the test, the grouting pressure reached 5.5 MPa, each test encompassed 1 m, and the average value over the three test boreholes was applied in each section. The segmented water injection experimental method was applied to analyse the overlying rock before and after mining, and the obtained data are shown in Fig. 3.

Figure 3 shows that the drilling water injection volume before mining is relatively small, essentially exhibiting a linear distribution, and the water injection volume is kept below 90 L/min, indicating that there are few primary fissures in the overlying rock before mining, and the degree of fissure development is low. The water injection volume curve of the rear drilling borehole exhibits a step-type distribution, and the water injection volume at a drilling depth of approximately 178 m returns to the level before mining. The water injection volume during the first drilling step ranges from 2200 to 2400 L/min, which is 24–26 times that before mining. The water injection rate during the second drilling step ranges from 1400 to 1500 L/min, which is 15–17 times that before mining. According to the development characteristics of fractures in the three zones in the overburden rock after mining combined with analysis of the water injection volume during drilling, the first step occurs in the collapse zone area, and the second step involves the fault zone area. The failure height of the drilling borehole is provided in Table 1. The development height of the collapse zone ranges from 38.8 to 40.2 m, and the development height of the fault zone ranges from 123.7 to 126.5 m.
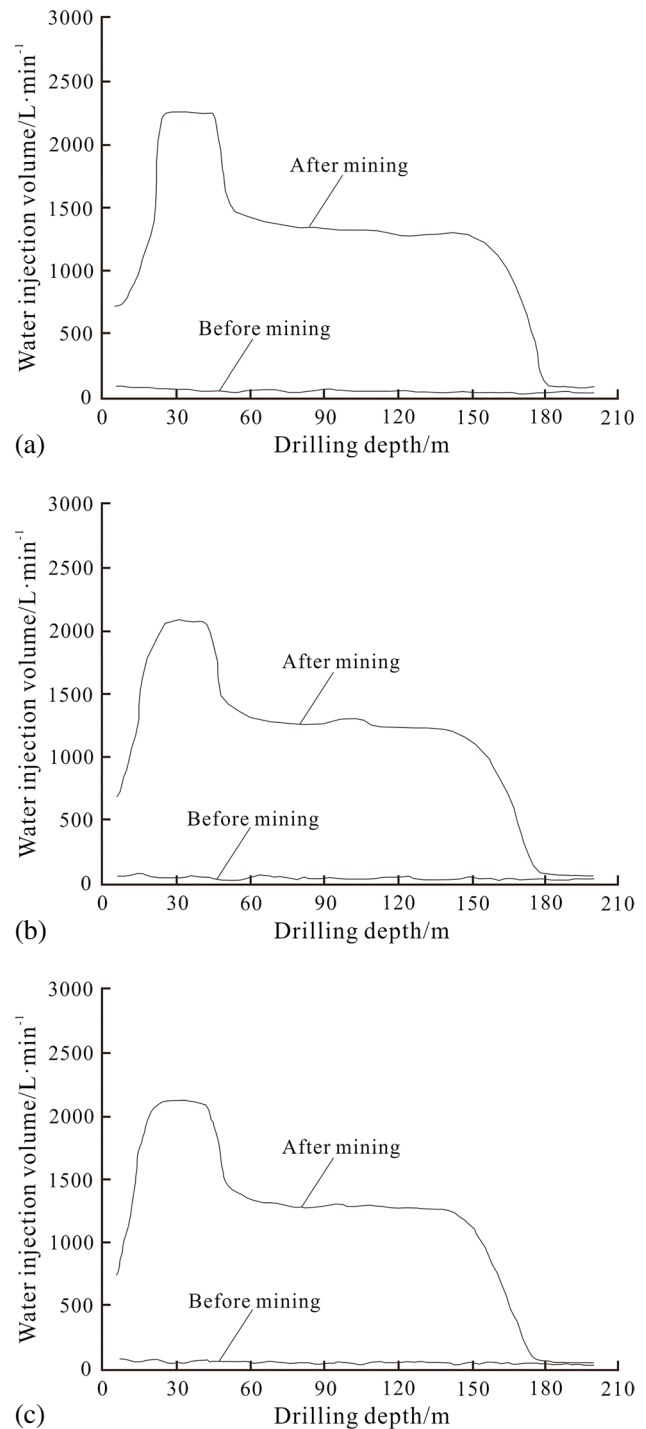
Fig. 3 Curves of the water injection rate (before and after mining). **a** Borehole number.Type equation here. **b** Borehole number. **c** Borehole number

Table 1 Failure height of the drilling borehole

Borehole number	Caving zone height	Height of the fractured water-conducting zone
	38.8 m	126.5 m
	40.2 m	125.8 m
	39.5 m	123.7 m

Microseismic monitoring technique

The microseismic monitoring technique is based on acoustic emission and seismology and has recently been developed into new types of high-tech monitoring techniques. Microseismic monitoring is a geophysical technique in which the impact and underground state of production activities are monitored by observing and analysing the small earthquakes generated. When underground rock ruptures and moves due to human or natural factors, a weak seismic wave is propagated. By arranging multiple sets of geophones in the space surrounding the rupture zone and collecting microseismic data in real time, the principle of vibration positioning can be applied to determine the rupture location and display it in three-dimensional space.

According to analysis of the overlying rock failure event characteristics and energy, the ARAMISM/E microseismic system is adopted, 10 sensors are arranged across the working face, and the sampling rate is set to 50 and 100, with a positioning accuracy of ± 50 m. Figure 4 shows the mining process of the working face. The overlying rock

microseismic conditions indicate a damage event with a measured energy release higher than 1000 J.

Figure 4 a shows that the working face advances 180–240 m, and the overburden failure height reaches 66 m. Figure 4b shows that the working face advances from 1080 to 1160 m, and the overburden failure height reaches 124–128 m at this time. The lower rock formations are all destroyed, with partial destruction of the upper rock formations. Based on the characteristics of overburden failure during advancement of the 4302 working face, it can be observed that with increasing advancement of the working face, the space of the mined-out area gradually increases, and the damage height of the overburden also gradually increases. With increasing working face advancement, the maximum height of overburden failure reaches 126 m.

Evolution characteristics of cracks in the overlying rock formations

The borehole TV technique is an important research method to observe the evolution of overlying rock cracks in coal seam mining. This technique relies on similar principles to those of CCD optical coupling for real-time acquisition of drilling borehole wall images, and through processing system transformation, a 360° image display of the borehole is generated. Moreover, depth imaging bit test system data used for real-time depth monitoring and transmission are sent to the processing system, forming images of the cracks in the borehole wall, as well as images of the fracture occurrence and measured depth. The borehole TV technique employs
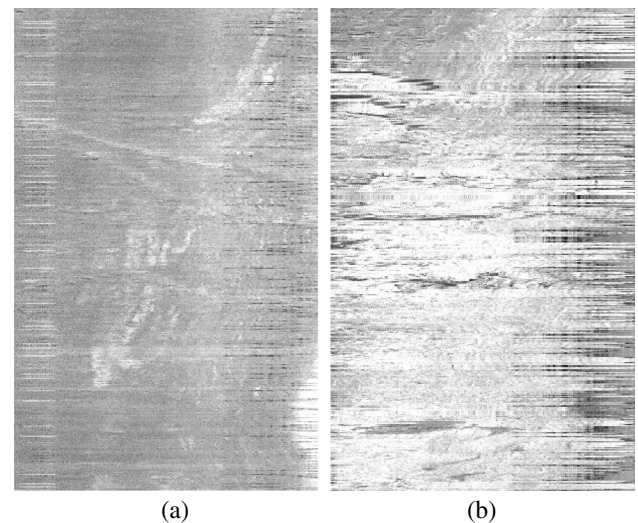

Fig. 4 Damage to the overburden during panel 4302 caving. **a** Mining distance (180–240 m). **b** Mining distance (1080–1160 m)

(a)   (b)
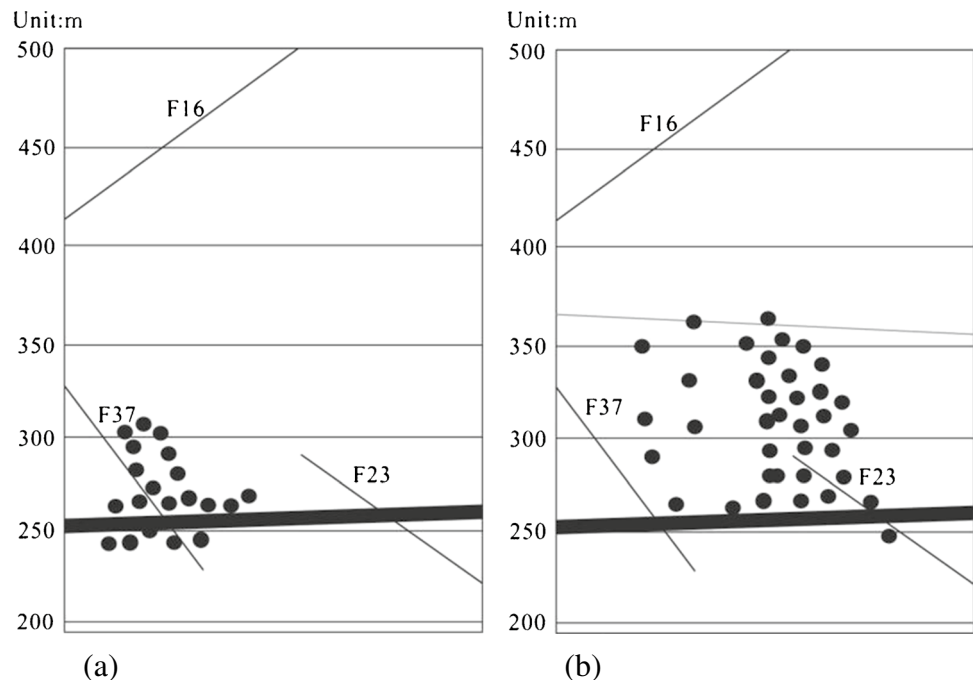
Fig. 5 Mechanism of borehole wall imaging
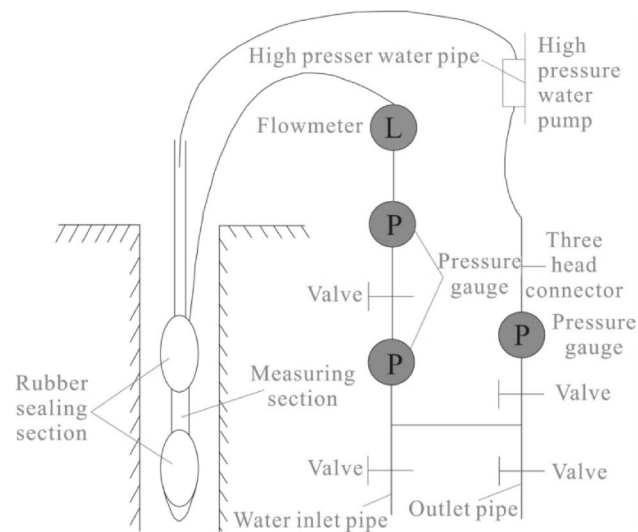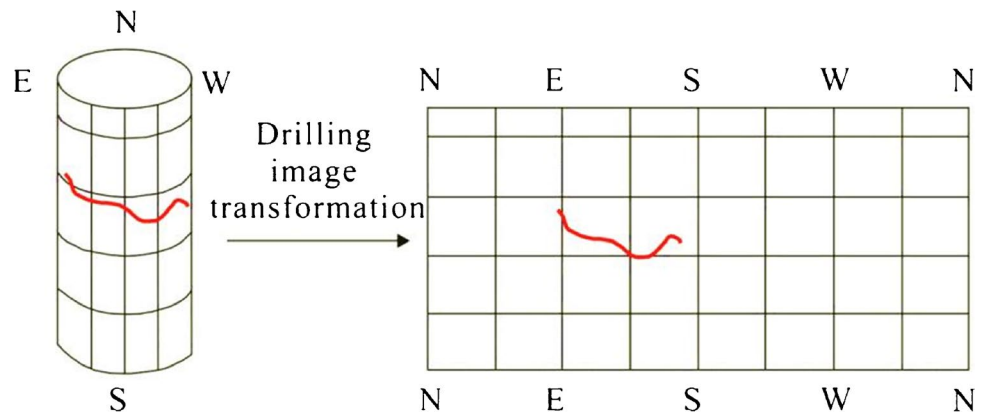
Fig. 6 Borehole TV system

Fig. 7 Fracture characteristics of the borehole wall before and after mining (11.0–11.5 m). **a** Before mining. **b** After mining

a computer to control image acquisition and processing and realize the transformation between modules and data. The imaging system is shown in Fig. 5, and the detection system is shown in Fig. 6.

The borehole TV method was applied to detect cracks in the overlying strata before and after movement of the mining face, and the detection results are shown in Fig. 7.

The borehole television detection data map shows that there are almost no cracks in the working face before mining, whereas cracks are clearly developed after mining. The characteristics of these cracks before and after mining are comprehensively analysed.

Distribution characteristics of the fracture dip angle

After vectorization processing of the borehole TV data map after detection, the inclination angle characteristics of the three boreholes are integrated, and the inclination angle distribution pattern is shown in Fig. 8.

Figure 8 shows that among the 42 fractures before mining, fractures with an inclination angle lower than 30° accounted for 7.14% of the total number of fractures, fractures with an inclination angle ranging from 30° to 39° accounted for 4.76% of all fractures, and fractures with an angle from 40° to 49° accounted for 9.52% of all fractures. Fractures with an inclination angle from 50° to 59° accounted for 9.52% of the total fractures, fractures with an inclination angle of 60° to 69° accounted for 26.19% of the total fractures, fractures with an inclination angle from 70° to 79° accounted for 23.81% of all fractures, and fractures with an inclination angle from 80° to 90° accounted for 9.52–19.05% of all fractures. It could be inferred that the premining fractures were dominated by high angles. Of the 102 fractures after mining, fractures with an inclination angle lower than 30° accounted for 14.71% of the total number of fractures, fractures with an inclination angle from 30° to 39°accounted for 23.53% of all fractures, and fractures with an inclination angle from 40° to 49° accounted for 20.59% of all fractures. Fractures with
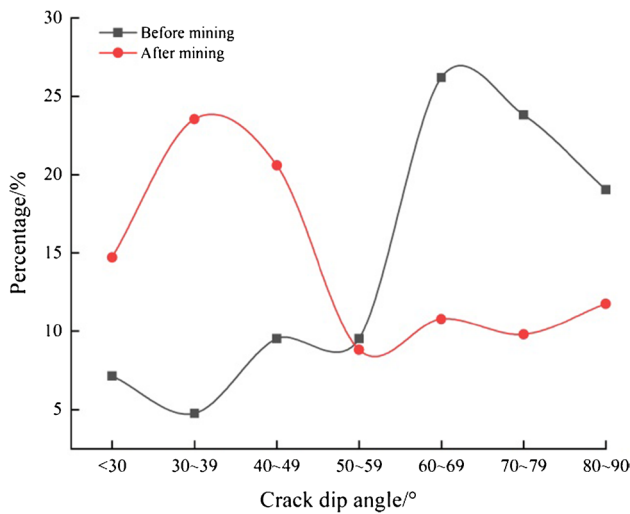
Fig. 8 Dip angle distributions of the fissures before mining and after mining

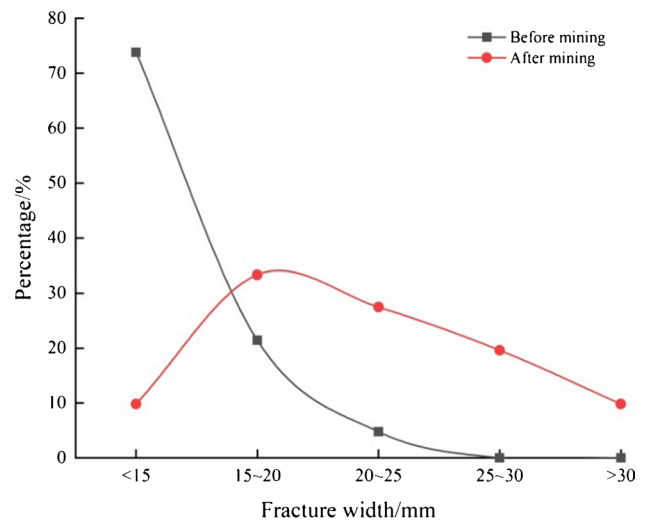Fig. 9 Distributions of the fracture width before and after mining

an inclination angle from 50° to 59°accounted for 8.82% of all fractures, fractures with an inclination angle from 60° to 69°accounted for 10.78% of all fractures, fractures with an inclination angle from 70° to 79° accounted for 9.80% of the total fractures, and fissures with an inclination angle from 80° to 90° accounted for 11.76% of the total fissures. It could be inferred that the newly formed fissures after mining mainly exhibited low angles.

Distribution characteristics of the fracture width

The fracture width reflects the degree of fracture development, and under the conditions of coal seam mining, the fracture width near the coal seam is markedly wider. Through the obtained statistics of the width of borehole fractures (Fig. 9), the fracture width before mining was mainly smaller than 15 mm, accounting for 73.81% of the total fractures, while after mining, the fracture width mainly ranged from 15 to 2 25 mm, accounting for 60.78% of the total fractures. The influence of mining could significantly increase the width of fissures in the overlying strata, which plays an important role in gas drainage and water prevention.

The change in the number of fissures can reflect the degree to which the rock mass is affected by mining. Figure 10 shows the relationship between the number of cracks and depth before and after mining.

A mountain-like distribution is observed before and after migration of the detected mining face fractures. The number of fractures in the overlying strata of the working face was small before mining. After mining, the number of fractures in the overlying strata affected by the mine working face was significantly increased, and the number of fractures first increased greatly with the drilling depth, but the number of

fractures began to decrease after the drilling depth reached approximately 56 m.

Similar simulations of the mining fracture evolution process

Similar simulations were conducted on the basis of the 4302 working face. The model size was 3000 mm × 2000 mm × 200 mm (length × width × height), a stress test bench was employed, fine sand was adopted for the aggregates, lime and gypsum were employed as cementing materials, and borax was applied as a retardant. Through the proportional test method, a mechanical experiment
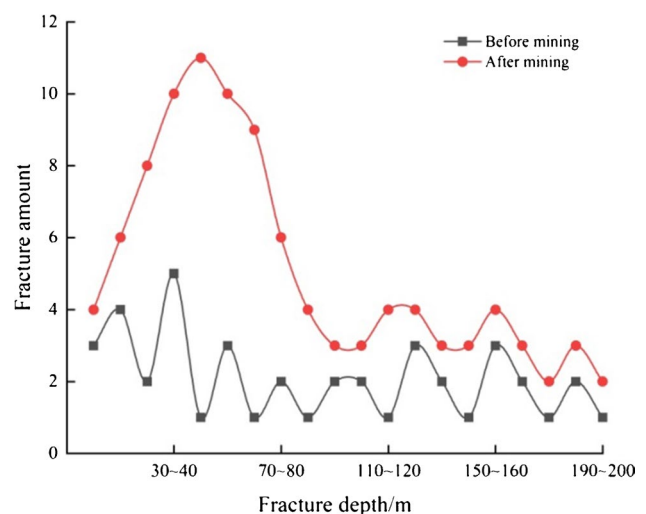
Fig. 10 Relationship curves between the drilling depth and number of fractures before and after mining operations

was conducted of the prepared structural material, and the mechanical requirements of similar simulation experiments were met.

Similar material simulations are based on the principle of similarity and comprise the theoretical basis of the three theorems of similarity. The first theorem of similarity was proposed by Newton in 1686 and rigorously demonstrated by French scientist J. Bertrand in 1848. The first theorem of similarity can be expressed as follows: when the similarity criterion of similar phenomena is equal, the similarity index value is 1, and the single-value conditions are similar. The characteristics of individual phenomena under single-value conditions are different from those of the same types of phenomena, which include geometric conditions, physical conditions, boundary conditions and initial conditions. Geometric conditions refer to the shape and size of the object participating in the process. Physical conditions refer to the physical properties of the object participating in the process, and initial conditions are the initial characteristics of the object. The second theorem of similarity was developed in 1911 by Russian scholar Feitelmann. The physical equations describing similar phenomena can be transformed into synthetic equations composed of similar quasi-numbers. If the observed phenomena are similar, the relationships among the parameters describing these phenomena can be transformed into functional relationships among the similarity criteria, and the comprehensive equations of similar phenomena must be the same. This theorem provides a theoretical basis for the generalization of similarity test results. If two phenomena are similar, the similarity criterion relationship can be developed into a prototype according to this theorem, and the prototype can be satisfactorily explained. The third theorem of similarity was established in 1930 by Kiir Pichev and Guhlman. In the geometric similarity system, two phenomena are similar if their equations with the same characteristics are similar under single-value conditions, and a similar number composed of single-valued conditions remain equal. According to the first theorem of similarity, the similarity criterion obtained from the model system can be extended to the original system in the model test method, and the test results obtained from the model can be applied to similar objects based on the second theorem of similitude. The third theorem of similarity points out the rules that must be followed when performing model tests. The geometric similarity ratio is 1:200, the bulk density ratio is 1.6, and the time similarity ratio is 14.1.

According to the similar simulation process, the final development height of the caving zone reaches 40.2 m, and the development height of the water-conducting fault zone is 124.8 m. The overlying rock exhibits an irregular trapezoidal shape and contains an arched structure at the open cut and coal wall. Moreover, the middle part of the goaf tends to be compacted, and the upper separation space is closed.

To visualize the failure characteristics of the overburden rock after mining, the crack density is adopted as an index to comprehensively analyse the characteristics of crack development, and a density curve of the number of cracks in the overburden rock under different distances of the working face is shown in Fig. 11.

Figure 11 shows the following crack density curve features: (1) during advancement of the working face, as the overburden collapses, cracks appear, and as the working face advances, the number and width of cracks gradually increase. (2) When the working face advances to a certain position, the overburden damage height can no longer increase with increasing advancement of the working face. Simultaneously, due to the presence of the overburden, the mined-out area can be compacted, and the number of cracks can decrease accordingly. The formation of characteristic fissures again varies. (3) In the area near the coal wall ahead of the working face, due to the occurrence of the supporting pressure, the number of cracks is large, and the density of the observed overburden cracks is distributed in a snake-like pattern.

Discussion

In the process of halting the advancement of the working face, fractures gradually developed from the bottom to the top under the influence of mining and formed various fracture network distributions under the different advancing distances. With continuous advancement of the working face, the immediate roof of the overlying strata began to collapse, while under the action of mining stress, the fractures on the left and right sides were extended towards the inner and outer sides of the goaf, respectively. With increasing advancement of the working face, the caving zone did not develop upwards, the central part of the mined-out area was compacted, the caving zone remained highly stable, and the original fracture network in the mined-out rock mass was altered. Simultaneously, new
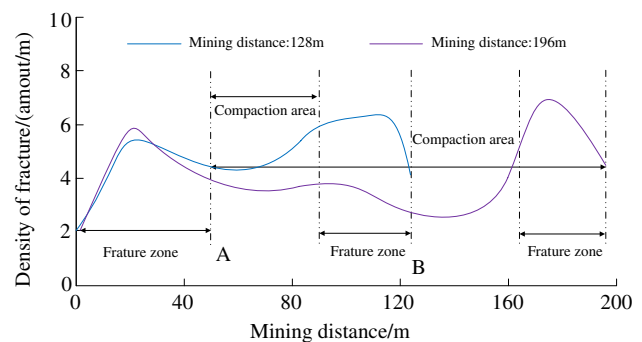

Fig. 11 Distribution pattern of the overlying fissure density

mining fractures were superimposed. As a result, the distribution of fractures in the rock mass of mining-induced coal became increasingly complex. When the working face was finished, the central part of the mined-out area was completely compacted, and the fractures were closed. Under the action of tensile stress, a large number of fractures either perpendicular or oblique to the bedding plane were produced. Mining plays an important role in promoting the development of cracks in the overlying strata.

Conclusion

With the application of borehole television observations, segmented water injection and microseismic monitoring technology were employed to detect the height of overburden failure in the mining process of the working face, quantitatively analyse the development of cracks in the mining process of the working face, and simulate the evolution characteristics of the observed cracks in combination with similar models. The following conclusions were obtained:

1) The development height of the caving zone in fully mechanized mining is 40.2 m, and the development height of the water-conducting fracture zone reaches 126.5 m. Digital analysis of the borehole television detection results indicates that the premining cracks are mainly high-angle and small-width cracks, the number of cracks linearly rises with gradual advancement of the coal mining face, and the newly formed cracks are small in length but mostly wide. At the early stages of mining, the number and width of cracks gradually increase with increasing advancement of the working face, but when the working face has advanced to a certain position, due to the occurrence of overlying strata, the mined-out area can be compacted, and the number of cracks can accordingly decrease. This compaction constantly features additional fissure changes.

2) During advancement of the working face, as the overburden collapses, cracks emerge, with the number and width size of these cracks gradually increasing, mostly in the area near the coal wall ahead of the working face, due to supporting pressure occurrence. While the number of cracks in the mine always remains large, the density of fissures in the overlying rock is distributed in a snaking pattern.

3) Because of the influence of working face mining, the development degree of overburden rock fractures is considerably increased, and a large number of fractures can greatly increase the permeability of the coal seam and improve the efficiency of gas extraction.

Declarations

References

Cai YD, Liu DM, Mathews JP, Pan ZJ, ElsworthYao YBm Li JQ, Guo XQ, D (2014) Permeability evolution in fractured coal combining triaxial confinement with x-ray computed tomography, acoustic emission and ultrasonic techniques. Int J Coal Geol 122(4):91–104

Cai YF, Li XJ, Deng WN, Xiao W, Zhang WK 2020 Simulation of surface movement and deformation rules and detriment key parameters in high-strength mining. J Min Strat Control Eng 2(4):043511

Cai MF 2020 Key theories and technologies for surrounding rock stability and ground control in deep mining. J Min

Chai J, Ou YYB, Zhang DD 2020a Crackdetection method in similar material models based on DIC. J Min Strat

Chai J, Ou YYB, Zhang DD, Lei WL 2020b Theoretical analysis of the mechanical coupling between rock and optical fiber for distributed sensing of overlying strata deformation. J Min Strat Control Eng 2(3):033038

Chen K, Ge Y, Zhang Q, Chen LF, Liu ZQ (2021) Discrete element simulation for crack fractal evolution laws associated with slicing mining in super thick coal stratum. J Eng Geo 29(4):1113–1120

Chen SL, Huang BX, Li D, Zhao XL, Xu J, Wang CW 2020 Experiment study on the basic law of high pressure abrasive hydraulic cutting for coal-rock mass. J Min Strat Control Eng 2(4):047521.

Chen J, Gao JK, Pu YY, Jiang DY, Qi QX, Wen ZJ, Sun QL, Chen LL 2021b Machine learning method for predicting and warning of rockbursts. J Min Strat Control Eng. 3(1):013026.

Chen JW 2020 Analysis of roadheader's rotary table on vibration modal based on finite element method and tested data. J Min Strat Control Eng 2(2):026032.

Cheng Z, Liu B, Zou Q, Wang X, Feng J, Zhao Z, Sun F (2019) Analysis of spatial–temporal evolution of mining-induced fracture field: a case study using image processing in the shaqu coal mine china. Nat Resour Res 29(3):1601–1615

Cheng JW, Zhao G, Sa ZY, Zheng WC, Wang YG, Liu J 2020 Overlying strata movement and deformation calculation prediction models for underground coal mines. J Min Strat Control Eng 2(4):043523.

Strat Control Eng 2(3):033037

Control Eng 2(2):023015.

Cui F, Jia C, Lai XP (2020) Study on the law of fracture evolution under repeated mining of close-distance coal seams. Energies 13(22):60–64

Du F, Wang WQ (2020) Li ZH (2020) Study on the evolution law of fracture field in full-mechanized caving mining of double system and extrathick coal seam. Advances in Civil Engineering 2:1–12

Ekin K (2020) Investigations on fracture evolution of coal measure sandstones from mineralogical and textural points of view. Indian Geotechnical Journal 50(6):1024–1040

Fan L, Liu SM (2019) Fluid-dependent shear slip behaviors of coal fractures and their implications on fracture frictional strength reduction and permeability evolutions. International Journal of Coal Geology 212(3):103235.

Fan K (2020) Sudden deformation characteristic and cuttingroof support technology for double-used roadways in Longtan Mine. J Min Strat Control Eng 2(3):033032.

Fang Y, Elsworth D, Wang CY, Jia YZ (2018) Mineralogical controls on frictional strength, stability, and shear permeability

evolution of fractures. Journal of Geophysical Research: Solid Earth 123(5):3549–3563

Feng J, Liu X, Yu Z (2017) Numerical simulation study on the mining-induced fracture evolution of steep coal seam. Journal of the China Coal Society 42(8):1971–1978

Fu X, Wang RF (2020) Cooperative self-adaptive control model of fluid feeding system and hydraulic supports in working face. J Min Strat Control Eng 2(3):036031.

Gan Q, Elsworth D, Zhao YX, Grippa A, Hurst A (2020) Coupled hydro-mechanical evolution of fracture permeability in sand injectite intrusions. Journal of Rock Mechanics and Geotechnical Engineering 12(4):742–751

Gao FQ 2019 Use of numerical modeling for analyzing rock mechanic problems in underground coal mine practices. J Min Strat Control Eng 1(1):013004.

Gao FQ 2021 Influence of hydraulic fracturing of strong roof on mining-induced stress-insight from numerical simulation. J Min Strat Control Eng 3(2):023032.

Gu H, Tao M, Cao W, Zhou J, Li X 2019 Dynamic frascture behaviour and evolution mechanism of soft coal with different porosities and water contents. Theoretical and Applied Fracture Mechanics 103(2):102265.

Han GL (2017) Grouting technique and water cut-off effect assessment of modified lake mud at Chengmenshan Copper Mine. Geotechnical Investigation and Surveying 45(11):13–17

He FL, Xu L, Wu HK, Wang YF (2014) Fracture field evolution and stability analysis of surrounding rock in thick coal roof large-section open-off cut. Journal of the China Coal Society 39(2):336–346

He YL, Gao MS, Xu D, Yu X 2021 Investigation of the evolution and control of fractures in surrounding rock under different pressure relief and support measures in mine roadways prone to rockburst events. Royal Society open science 8(3): 202044.

Hou EK, Cong T, Xie XS, Wei JB 2020a Ground surface fracture development characteristics of shallow double coal seam staggered mining based on particle flow. J Min Strat Control Eng 2(1):013521.

Hou JF, Guo ZP, Liu WZ, Yang HZ 2020b Study on damage model and damage evolution characteristics of backfill with prefabricated fracture under seepage-stress coupling.Advances in Materials Science and Engineering 2020b(1):1–11.

Hu YB, Li WP, Wang QQ, Liu SL, Wang ZK (2019) Evolution of floor water inrush from a structural fractured zone with confined water. Mine Water Environ 38(2):252–260

Hu QF, Cui XM, Liu WK, Ma TJ, Geng HR 2020 Law ofoverburden and surface movement and deformation due to mining super thick coalseam. J Min Strat Control Eng 2(2):023021

Hu QT, Jiang ZZ, Li QG, Wu WB, Wang QG, Wang XG, Ran YJ, Tong SL 2021 Induced stress evolution of hydraulic fracturing in an inclined soft coal seam gas reservoir near a fault. Journal of Natural Gas Science and Engineering 88(4):103794.

Huang QM, Wu B (2018) Evolution of the fractured zone above a coal face with a large mining height: a case study of the Dahuangshan Coalmine China. Geotech Geol Eng 36(6):3559–3571

Huang QL, Yuan Y, Yu L (2015) Evaluation of hot bitumen grouting on voids of semi-rigid base. Journal of Transport Science and Engineering 31(3):13–17

Huang FR, Yan SX, Wang XL, Jiang PC, Zhan SB 2021 Experimental study on infrared radiation characteristics of gneiss under uniaxial compression. J Min Strat Control Eng. 3(1):013011.

Jia YZ, Lu YY, Tang JR, Fang Y, Xia BW (2018) Ge ZL (2018) Mechanical-chemical-mineralogical controls on permeability evolution of shale fractures. Geofluids 4:1–18

Jia C, Hu CC 2020 Instability mechanism and control technology of longwall entries driving along the gob in a thick coal seam. J Min Strat Control Eng 2(4):043535.

Jiang KG, Wang L, Chi SS, Wei T, Jiang C 2021 Boltzmann function prediction model coupled with the correction of inflection point offset and its parameter inversion method. J Min Strat Control Eng 3(2):023527.

JiangG ZJ, Sun B, Ping Y, Zhu ZD 2021 Experimental on dynamic response characteristics of rock based on large diameter SHPB. J Min Strat Control Eng, 2021, 3(4):043021.

Ju Y, Wang Y, Ren Z, Mao L, Wang Y, Chang FP 2020 Optical method to quantify the evolution of whole-field stress in fractured coal subjected to uniaxial compressive loads. Optics and Lasers in Engineering 128(6):106013.

Kang HP 2020 Spatial scale analysis on coalmining and strata control technologies. J Min Strat Control Eng2(2):023538.

Kang HP 2021 Temporal scale analysis on coal mining and strata control technologies. J Min Strat Control Eng.3(1):013538.

Li JH, Sun GL, Su PL, Gu SC (2017) Test study on dynamic water grouting sedimentary pressure characteristics and grouting effect. Mining Safety and Environmental Protection 44(6):21–24

Li Y, Du G (2020) Reasonable width of narrow coal pillars in roadway driving with gas drainage hole. J Min Strat Control Eng 2(1):013007

Li JK, Wang H 2020 Ground support of interbedded rock roof in a deep roadway with fully-anchored cables. J Min Strat Control Eng 2(3):033036

Li JH, Li HJ, Li ZC, Wu ZQ 2020a Research on river dike failure of short-distance coal seams mining under Hunchun River. J Min Strat Control Eng 2(1):013538.

Li YP, Cui F, Yang WH, Wei CXQ 2020b Dynamic migration law and its control of roof in fully mechanized top coal caving mining in extremely steep and thick coal seams. J Min Strat Control Eng 2(4):043538.

Li HG, Li HM, Xu GS 2021a Influence of water content on mechanical characteristics of weakly cemented sandstone. J Min Strat Control Eng 3(4): 043029.

Li JY, Wang L, Jiang KG, Teng CQ 2021b Parameter inversion method of probability integral model based on improved wolves algorithm. J Min Strat Control Eng. 3(1):017038.

Liu J, Wang J (2018) Stress evolution of rock-like specimens containing a single fracture under uniaxial loading: a numerical study based on particle flow code. Geotech Geol Eng 36(1):567–580

Liu ZH, Liu JS, Pan PZ, Derek E, Wei MY, Shi R (2020) Evolution and analysis of gas sorption-induced coal fracture strain data. Pet Sci 17(2):376–392

Liu SP, Wan P, Wan ZJ, Lv JK, Lu SF, Wang YC 2021 Analysis of coal wall vibration. J Min Strat Control Eng.3(3): 033514.

Ma ZQ, Jiang YD, Du WS, Zuo YJ, Kong DZ (2018) Fracture evolution law and control technology of roadways with extra thick soft roof. Eng Fail Anal 84(3):331–345

Ma WZ, Zhou XM, Tan S 2020 Study on failure characteristics of coal seam floor above confined water: a case study of Shanxi Yitang Coal Mine. J Min Strat Control Eng 2(3):033011.

Miao G, Li Z, Sun L, Yang Y (2019) Experimental study on pore-fracture evolution law in the thermal damage process of coal. Combust Sci Technol 193(4):677–701

Ni GH, Xie HC, Li S, Sun Q, Huang DM, Cheng YY, Wang N (2019) The effect of anionic surfactant (SDS) on pore-fracture evolution of acidified coal and its significance for coalbed methane extraction. Adv Powder Technol 30(5):940–951

Pan RK, Fu D, Yu MG, Chen L (2017) Directivity effect of unloading bedding coal induced fracture evolution and its application. Int J Min Sci Technol 27(5):825–829

Pan H, Zhu L, Zhang XF, Gu WZ, Liu ZC, Li J, Song TQ, Qiu FQ 2020 Distribution characteristics of deviatoric stress and control technology of surrounding rock at temporary water chamber group in deep mining. J Min Strat Control Eng 2(4):043033.

Qie L, Shi YN, Liu JG 2021 Experimental study on grouting diffusion of gangue solid filling bulk materials. J Min Strat Control Eng 3(2):023011.

Ren YF 2020 Analysis and evaluation method for supporting ability of supports in coalmine working face. J Min Strat Control Eng 2(3):036012.

Shi LQ, Xu DJ, Wang Y, Qiu M, Hao J (2019) A novel conceptual model of fracture evolution patterns in the overlying strata during horizontal coal seam mining. Arab J Geosci 12(10):1–12

Su FQ, Yu GL, Guo XC, Fan WT, Jing SJ, Pu H, Wl W (2020) Study on internal structure change and model test of coal samples in thermal environment based on underground coal gasification. Journal of the China Coal Society 45(12):4191–4200

Su SL, Du Y, Zhu JF, Zhang L, Zhao ZL, Meng B 2020b Numerical study on bearing behavior of layered rock mass for deep roadway. J Min Strat Control Eng 2(1):013002.

Su QQ, Ma QY, Ma DD, Yuan P 2021 Dynamic mechanical characteristic and fracture evolution mechanism of deep roadway sandstone containing weakly filled joints with various angles. International Journal of Rock Mechanics and Mining Sciences 137(4):104552.

Tang J, Zhu J, Shao TS, Wang JG, Jiang YD (2021) A coal permeability model with variable fracture compressibility considering triaxial strain condition. Nat Resour Res 30(2):1577–1595

Trofimov VA, Shipovskii IE (2020) Computer modeling of coal seam blasting. J Min Sci 56(5):741–752

Wang XL (2019) Research status and development tendency of the height of cover rock destruction after seam mining. Science Technology and Engineering 19(2):1–10

Wang SG, Elsworth D, Liu JS (2011) Permeability evolution in fractured coal: the roles of fracture geometry and water-content. Int J Coal Geol 87(1):13–25

Wang J, Wang XL 2021 Seepage characteristic and fracture development of protected seam caused by mining protecting strata. J Min Strat Control Eng. 3(3):033511.

Wang GF, Pang YH, Ren HW 2020a Intelligent coal mining pattern and technological path. J Min Strat Control Eng 2(1):013501.

Wang J, Zhang C, Zheng D, Song WD, Ji XF 2020b Stability analysis of roof in goaf considering time effect. J Min Strat Control Eng 2(1):013011

Wang Y, Tu M, Fu BJ, Bu QW 2020c Lateral mining-induced stress distributive property of deep mining and gob-side entry support. J Min Strat Control Eng 2(3):033012.

Wang DL, Hao BY, Liang XM 2021 Slurry diffusion of single fracture based on fluid-solid coupling. J Min Strat Control Eng. 3(1):013038

Wang JC 2019a Sustainable coal mining based on mining ground control. J Min Strat Control Eng 1(1):013505.

Wei MY, Liu JS, Liu YK, Liu ZH, Elsworth D (2021) Effect of adsorption-induced matrix swelling on coal permeability evolution of micro-fracture with the real geometry. Pet Sci 18(4):1143–1152

Wei MY, Liu JS, Elsworth D, Liu YK, Zeng J, He ZH 2021a Impact of equilibration time lag between matrix and fractures on the evolution of coal permeability. Fuel 290(1):120029.

Wu JW, Shen SH, Zhai XR, Wei DY, Zhang PS, Han YC (2014) The wave velocity detection and evaluation of the effect of grouting reinforcement in coal seam floor. Geophysical and Geochemical Exploration 38(6):1302–1306

Wu WD, Bai JB, Wang XY, Zhu ZJ, Yan S (2019) Field investigation of fractures evolution in overlying strata caused by extraction of the jurassic and carboniferous coal seams and its application: case study. Int J Coal Geol 208(3):12–23

Wu MY, Wang WS, Zhang DM, Deng BZ, Liu SM, Lu J, Luo YF, Zhao WC 2021 The pixel crack reconstruction method: from fracture image to crack geological model for fracture evolution simulation. Construction and Building Materials 273(2): 121733.

Xia YX, Lu C, Yang GY, Su SJ, Pang LN, Ding GL, Su B 2020 Experimental study on axial fracture cutting and fracturing of abrasive jet in hard roof hole. J Min Strat Control Eng 2(3):033522.

Xia YX, Feng MH, Wang SW, Lu C 2021 Risk assessment method of rock burst based on the combination of theory and field detection. J Min Strat Control Eng, 2021, 3(4): 043017.

Xiao GG, Yao WB 2021 Law of pressure behavior of shallow buried coal seam in the gully terrain of Madiliang Coal Mine. J Min Strat Control Eng, 2021, 3(4):043023.

Xie ZZ, Zhang N, Feng XW, Liang DX, Wei Q, Weng MY (2019) Investigation on the evolution and control of surrounding rock fracture under different supporting conditions in deep roadway during excavation period. Int J Rock Mech Min Sci 123(4):104–122

Xu NZ, Gao C 2020 Study on the special rules of surface subsidence affected by normal faults. J Min Strat Control Eng 2(1):011007.

Xu JL, Xuan DY, Zhu WB, Wang XZ 2019 Partial backfilling coal mining technology based on key strata control. J Min Strat Control Eng 1(1):013504.

Xue JH, Wang HP, Zhou W, Ren B, Duan CR, Deng DS (2016) Erratum to: Experimental research on overlying strata movement and fracture evolution in pillarless stress-relief mining. International Journal of Coal Science and Technology 3(3):350–354

Yan H, Tan LP, Feng RM, Mitri H, Chen JZ (2020) Fracture evolution in coalbed methane reservoirs subjected to liquid nitrogen thermal shocking. Journal of Central South University 27(6):1846–1860

Yang DF, Zhang YJ, Wang S, Niu CH, Chai JL 2020a Analysis of the influence of hidden fault dip angle on ground pressure behavior in shallow seam roof. J Min Strat Control Eng 2(4):043038

Yang GH, Wang K, Zhang XQ 2020b Study on non-pillar mining technology of preset packing body and roof cutting in deep well roadway. J Min Strat Control Eng 2(1):013038.

Ye Q, Wang WJ, Wang G, Jia ZZ (2017) Numerical simulation on tendency mining fracture evolution characteristics of overlying strata and coal seams above working face with large inclination angle and mining depth. Arab J Geosci 10(4):1–15

Yin GZ, Li X, Han PB, Li MH, Li WP, Deng BZ (2016) Experimental study on overburden strata fracture evolution law in three dimensional mine-induced stress conditions. Journal of the China Coal Society 41(2):406–413

Yin GZ, Shang DL, Li MH, Huang J, Gong TC, Zl S, Deng BZ, Liu C, Xie ZC (2018) Permeability evolution and mesoscopic cracking behaviors of liquid nitrogen cryogenic freeze fracturing in low permeable and heterogeneous coal. Powder Technol 325(6):234–246

Yu XY, Wang ZS, Yang Y, MaoXW 2021 Numerical study on the movement rule of overburden in fully mechanized caving mining with thick depth and high mining height. J Min Strat Control Eng 3(1):013533

Yuan P, Xu Y (2019) Analyses on deformation and fracture evolution of zonal disintegration during axial overloading in 3D geomechanical model tests. Journal of Vibroengineering 21(4):1163–1174

Zhai YH (2015) Grouting water sealing technology for mine shaft sinking through water bearing goaf. Coal Engineering 47(2):41–43

Zhai JH, Ren S, Wang FT, Bi CG, Niu TC, Li Z 2022 Response law of ground pressure behavior and gas migration in fully mechanized topcoal caving mining. J Min Strat Control Eng 4(1):013013.

Zhang WX, Liu HL, Xie QY (2014) Affected factors analysis of pile foundation grouting reinforcing effect in karst region. Railw Eng 20(7):28–30

Zhang T, Wang YL (2020) Study on deformation evolution law and support technology of surrounding rock in multiple mining roadway. J Min Strat Control Eng 2(2):023016.

Zhang N, Han CL, Xie ZZ 2019 Theory of continuous beam control and high efficiency supporting technology in coal roadway. J Min Strat Control Eng 1(1):013005.

Zhang BL, Shen BT, Zhang JH, Zhang XG 2020a Experimental study of edge-opened cracks propagation in rocklike materials. J Min Strat Control Eng 2(3):033035.

Zhang C, Song WD, Fu JX, Li Y, Zhang KC 2020b Technology for roadway management of fractured rock masses in a submarine gold mine. J Min Strat Control Eng 2(3):033039.

Zhang GJ, Yan W, Jiang KG 2021 Inversion method for the prediction parameters of mining subsidence based on the PB combination prediction model of variable weight. J Min Strat Control Eng. 3(1):013524.

Zhao QC, Fu BJ 2020 Study on loose zone testing and support technology of roadway surrounding rock affected by dynamic pressure. J Min Strat Control Eng 2(2):023031.

Zhou X, Liu SM, Zhang YD (2021) Permeability evolution of fractured sorptive geomaterials: a theoretical study on coalbed methane reservoir. Rock Mech Rock Eng 54(7):3507–3525

Zhu J, Tang C, Hou CY, Shao TS, Zhao YH, Wang JG, Lin L, Liu LL, Jiang YD (2021) Two-phase flow model of coalbed methane extraction with different permeability evolutions for hydraulic fractures and coal reservoirs. Energy Fuels 35(11):9278–9293

Zhu W, Teng YH 2021 Study on the safety and mining influence of fully-mechanized caving mining with ultrathick seam under barrier lake. J Min Strat Control Eng. 3(1):013525.

Zhu WC, Niu LL, Li SH, Li S 2019 Creep-impact test of rock: status-of-the-art and prospect. J Min Strat Control Eng 1(1):013003.

Zuo JP, Yu ML, Hu SY, Song HQ, Wei X, Shi Y, Zuo SH 2019 Experimental investigation on fracture mode of different thick rock strata. J Min Strat Control Eng 1(1):013007.